Langmuir

ARTICLE

pubs.acs.org/Langmuir

Direct Submolecular Scale Imaging of Mesoscale Molecular Order in Supported Dipalmitoylphosphatidylcholine Bilayers

Khizar H. Sheikh,* Cristiano Giordani, Jason I. Kilpatrick, and Suzanne P. Jarvis

Nanoscale Function Group, Conway Institute of Biomolecular and Biomedical Research, University College Dublin, Belfield, Dublin, Ireland

ABSTRACT: Supported dipalmitoylphosphatidylcholine (DPPC) bilayers are widely used membrane systems in biophysical and biochemical studies. Previously, short-range positional and orientational order of lipid headgroups of supported DPPC bilayers was observed at room temperature using low deflection noise frequency modulation atomic force microcopy (FM-AFM). While this ordering was supported by X-ray diffraction studies, it conflicted with diffusion coefficient measurements of gel-phase bilayers determined from fluorescence photobleaching experiments. In this work, we have directly imaged mica-supported DPPC bilayers with submolecular resolution over scan ranges up to 146 nm using low deflection noise FM-AFM. Both orientational and positional molecular ordering were observed in the mesoscale, indicative of crystalline order. We discuss these results in relation to previous biophysical studies and propose that the mica support induces mesoscopic crystalline order of the DPPC bilayer at room temperature. This study also demonstrates the recent advance in the scan range of submolecular scale AFM imaging.

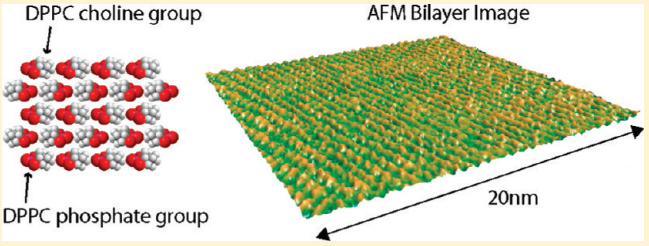

INTRODUCTION

Model lipid membranes have been used in biophysical and biochemical studies for many years. Dipalmitoylphosphatidylcholine (DPPC) bilayers in particular have been used as model systems for structural and physical studies using techniques such as differential scanning calorimetry, neutron diffraction and reflectivity, X-ray diffraction, and fluorescence recovery after photobleaching (FRAP). These studies have identified and characterized several bilayer phases, which in order of hydration include a crystalline "subtransition" L_c phase,[1−3] the $L_{\beta'}$ gel phase, the pretransition $P_{\beta'}$ (ripple) phase, and the liquid crystalline L_α or fluid phase. These phases are characterized by the degree of positional and orientational ordering of the hydrocarbon chains of the lipid molecules. The liquid crystal fluid bilayer phase is characterized by orientational ordering roughly perpendicular to the bilayer plane only. The gel phase additionally exhibits orientational order in the bilayer plane, and the crystalline phases additionally exhibit positional ordering in the bilayer plane. The lipid headgroups are considered to be ordered only in crystalline phases.

Although there is generally good agreement between the structural studies, there are some seemingly contradictory results. For example, FRAP measurements of lateral diffusion coefficients in DPPC bilayers at ca. 25 °C are approximately 10^{-11} cm^2/s,[4,5] suggesting only transient short-range in-plane ordering. In contrast, a wide-angle X-ray diffraction study of "gel" phase DPPC bilayers at the same temperature indicated that positional ordering in the bilayer plane extends to about 300 nm.[6]

The recent development of low deflection noise frequency modulation atomic force microcopy (FM-AFM) has enabled the direct imaging of surfaces in liquid environments with atomic resolution and piconewton force sensitivity.[7] Previously in this group, we imaged the short-range ordering of phospholipid headgroups in mica-supported DPPC bilayers at 21 °C.[8,9] Unresolved questions that remained were, over what range did this order persist, and how could this ordering be reconciled with finite lateral diffusion coefficients?

Improvements in fluid cell stability and the frequency modulation (FM) feedback system[10] have now enabled us to extend submolecular resolution imaging to hundreds of nanometers, and we now report results here that show that the molecular ordering in mica-supported DPPC bilayers at 23 °C exists not just over a few nanometers but up to at least 146 nm. We show defects in the bilayer structure and discuss the results in context with previous structural and biophysical studies.

EXPERIMENTAL SECTION

Sample Preparation. 1,2-Dipalmitoyl-*sn*-glycero-3-phosphocholine (DPPC) was purchased from Sigma-Aldrich and solubilized in chloroform (Sigma-Aldrich) at a stock concentration of 5 mM; 140 μL of stock solution was dried under an argon flow for 30 min and vacuum desiccated for 90 min to remove traces of solvent. The sample was hydrated by vortexing with 1 mL of phosphate-buffered saline (PBS) at pH 7.4 (0.01 M phosphate buffer, 0.0027 M potassium chloride and 0.137 M sodium chloride, Sigma-Aldrich) for 5 min at 55 °C. The vesicle suspension was tip sonicated (Hielscher Ultrasonics GmbH, UPH50) for 20 min at 55 °C to generate small unilamellar vesicles (SUVs). The sample was centrifuged at 10 000 rpm for 5 min and the supernatant

Received: November 23, 2010
Revised: January 31, 2011
Published: March 03, 2011

collected to remove metal particulates generated during tip sonication. Bilayers were prepared by incubation of freshly cleaved mica substrates (15 mm diameter, SPI Supplies Inc.) with 100 μL of SUV suspension at a temperature of 55 °C (above the main chain melting transition temperature for DPPC bilayers to promote continuous bilayer formation) in a humidified enclosure. Samples were rinsed by fluid exchange (10 times with 100 μL) with PBS and equilibrated for 1 h in the AFM fluid cell prior to imaging.

AFM Imaging. Amplitude modulation (AM) AFM images were taken using an MFP-3D-SA AFM (Asylum Research Inc.) at 26 ± 1 °C using SNL cantilevers (Veeco Instruments Ltd.) excited at a frequency of 20.4 kHz with a 12 nm peak free oscillation amplitude and 1.6 nN time-averaged imaging force. The optical lever sensitivities of the cantilevers were determined by force measurements against freshly cleaved mica surfaces. Spring constants were determined by the fitting of thermal oscillatory amplitude spectra with a simple harmonic oscillator model using the method of Hutter and Bechhoefer,[11] built into the software of the MFP-3D-SA AFM.[12] The imaging force was calculated from the difference between the free oscillation amplitude and the imaging amplitude set point.

FM-AFM imaging was performed at 23 ± 1 °C using a custom-built low deflection noise AFM, details of which have been previously published.[7] SSS-NCH-AuD silicon cantilevers (Windsor Scientific Ltd.) were used, excited in the second flexural mode at a frequency of ca. 880 kHz with a constant oscillation amplitude of 1.85 Å and a time-averaged imaging force of ca. 35 pN. The imaging force was derived from the frequency shift set point using the algorithm by Sader and Jarvis.[13]

It has been shown that use of small cantilever oscillation amplitudes is an effective means of increasing lateral resolution in FM-AFM imaging due to an increase in sensitivity to short-range interaction force gradients.[14] Operation with such small oscillation amplitudes often requires the use of cantilevers with high spring constants in order to reduce the magnitude of deflection noise arising from the thermal motion of the cantilever. Previously, higher cantilever flexural modes have been employed as a practical means of accessing small amplitude FM-AFM as a result of significant increases in the dynamic cantilever spring constants associated with these modes.[15,16] It should be noted that operating on the fundamental mode of a cantilever with stiffness equivalent to that of the flexural mode used in this study should yield the same performance.

Images were first- or second-order line-flattened but otherwise are not filtered or averaged.

RESULTS AND DISCUSSION

Figure 1A shows a 4 μm square image of a DPPC bilayer on mica at a temperature of 26 °C in PBS buffer at pH 7.4 taken in AM mode, the magnification and resolution being typical for lipid bilayer imaging using current commercial AFMs.[17] The crystalline nature of the bilayer is evident by the cracking of the bilayer into micrometer-sized domains during cooling. Defects formed at the domain edges suggest a bilayer thickness of 4.85 nm. This is consistent with the saturated lipid acyl chains being in a predominantly extended (trans) conformation and is in good agreement with previous AFM studies of DPPC bilayers.[18,19] Neutron diffraction and reflectivity studies have also shown DPPC bilayer thicknesses of about 4 nm with an underlying water layer of about 1 nm.[20,21] Figure 1B shows a slightly higher (×8.2) magnification image of a DPPC bilayer imaged using low deflection noise FM-AFM. In this case the imaging force is approximately 40 times lower, substantially reducing the tip−sample interaction force and allowing picometer height variations, such as the striations (running top left to bottom right of the image) arising from steps in the bilayer topography, to be seen. A single large defect of 1 nm depth and two smaller defects

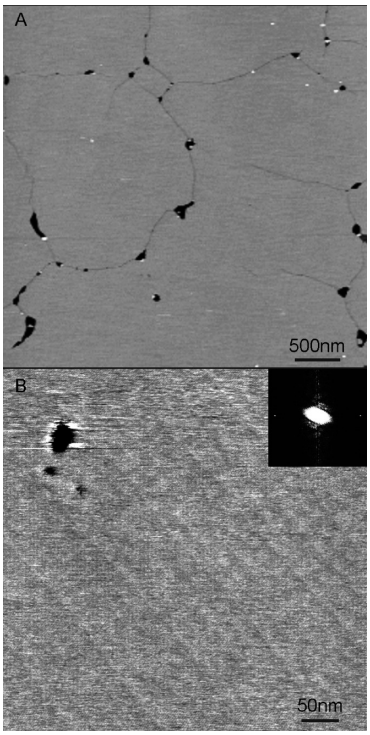

Figure 1. DPPC bilayer in PBS buffer: (A) 4 μm × 4 μm AM-AFM image, tip velocity 9.28 μm/s, *z*-scale 5 nm (black to white), and 15.6 nm pixel width and (B) 582 nm × 490 nm low deflection noise FM-AFM image, *z*-scale 150 pm, tip velocity 2.84 μm/s, and 1.1 nm pixel width. Defects of nanometer-scale depth are seen in both images.

10−15 nm in diameter and with a depth of about 100−150 pm can be seen. The nature of these defects cannot be determined topographically but are likely to arise from small surface contaminants that prevent spreading of the distal bilayer leaflet over this area during bilayer formation. The pixel width of the image is 1.1 nm and therefore too high to directly resolve molecular resolution information; nevertheless, faint aliasing peaks with 6.3 nm periodicity are seen in the inset FFT image, indicative of underlying order.

Figure 2 shows a 146 nm × 61 nm scan of the DPPC bilayer with 0.14 nm pixel width. At this magnification and imaging resolution, molecular headgroup ordering can just be resolved in the real space image. A comparison of the trace and retrace images [the surface is raster scanned, and height data of the left-to-right (trace) scan and right-to-left (retrace) scan of the same line are acquired] shows that headgroup ordering is seen in both scans, with orthorhombic lattice order confirmed in both of the inset FFTs. Other small variations in surface topography such as that circled in Figure 2A are also seen, and as these are not mirrored in trace and retrace scans, they represent imaging artifacts. The striations seen in Figure 1B are also seen in both scans of this image and run diagonally left to right (between arrows in Figure 2A). The origin of such small 10−15 pm steps in the bilayer topography is unknown.

Figure 3 shows a higher magnification scan with a pixel width of 0.2 nm encompassing the two smaller bilayer defects seen in Figure 1B. At this magnification and resolution, the molecular ordering can clearly be resolved, with rows of molecular headgroups seen to run diagonally left to right. The progressive breakdown of lattice structure in the vicinity of the bilayer defects can

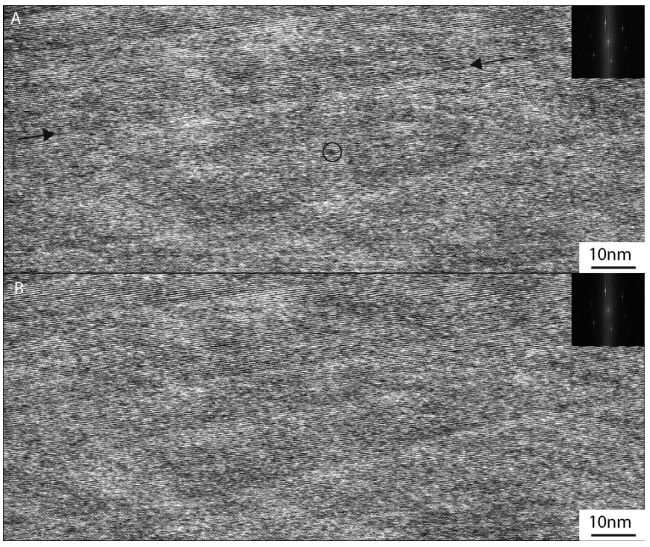

Figure 2. A 146 nm × 61 nm low deflection noise FM-AFM image of DPPC bilayer in PBS buffer, with tip velocity 711 nm/s, *z*-scale 75 pm (black to white), and 1.4 Å pixel width: (A) the trace image and (B) the retrace image of the same scan (see text). Lipid headgroup ordering is just evident on the real space and clearly evident on the inset FFT images.

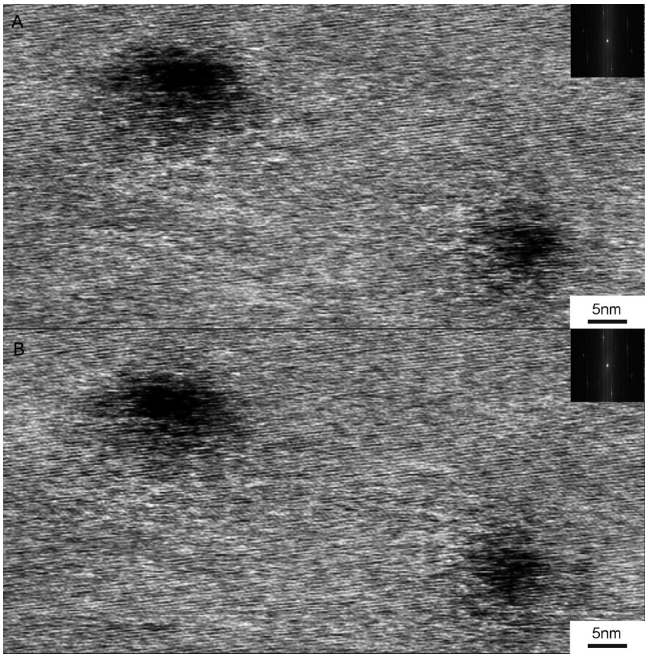

Figure 3. A 83 nm × 42 nm low deflection noise FM-AFM image of DPPC bilayer in PBS buffer, with tip velocity 493 nm/s, *z*-scale 150 pm (black to white), and 2 Å pixel width. The image shows the same two small defects identified in Figure 1B, and the molecular headgroup ordering is clearly visible. The breakdown of lattice order can be seen at the defect edges with some rows of lipid headgroups bridging the defect edges.

clearly be seen. Orthorhombic order is again confirmed in the inset FFT images.

Figure 4A,B shows higher magnification scans of the lipid headgroups. The headgroups can be seen to be composed of an ordered array of protrusions of diameter 4.0 ± 0.5 Å. Analysis of

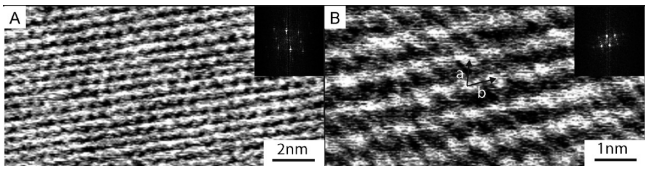

Figure 4. Low deflection noise FM-AFM images of DPPC bilayer in PBS buffer with increased magnification, *z*-scale 50 pm (black to white): (A) 15 nm × 7.5 nm, tip velocity 91 nm/s, and 0.7 Å pixel width and (B) 8 nm × 4 nm, tip velocity 46 nm/s, and 0.4 Å pixel width. The lattice order of the phosphate and choline moieties of the headgroups is clearly evident, and the lattice vectors are annotated.

the FFT images indicates that the orthorhombic lattice formed by the lipid headgroups have two-dimensional lattice vectors of $a = 4.6 \pm 0.3$ Å and $b = 5.6 \pm 0.6$ Å and an angle of $61.4 \pm 2.1°$. The dimensions of these features are consistent with being associated with the phosphate and choline moieties of the lipid headgroups. This assignment is in agreement with neutron diffraction studies[20] and with atomistic models[22] of DPPC bilayers showing that the choline headgroups are oriented almost parallel to the plane of the bilayer, thereby forming surface electric dipoles.

It should also be noted that at the scanning rates of the experiments (a few seconds per headgroup), the topography represents the time-averaged position of the headgroup moieties. Due to the variation in the size and separation of the headgroup moieties, it was not possible to unequivocally assign individual phosphate and choline moieties. On the basis of the observed order and also from theoretical modeling of phosphatidylcholine headgroup organization,[23] it is proposed that the surface electric dipoles align to form an ordered two-dimensional lattice schematically illustrated in Figure 5. On the basis of this model the molecular unit cell vector is twice that of lattice vector *b*.

The unit vectors allow the area per molecule of 45 ± 15 Å^2 to be calculated, and this value compares favorably with those determined from monolayer pressure−area isotherms,[24] wide-angle X-ray scattering experiments,[6,25] and molecular dynamics simulations.[26]

The DPPC lipids in the bilayer are therefore special cases of liquid crystals, with a director associated with the acyl chains roughly perpendicular to the bilayer surface and a second director, associated with the headgroup dipole aligned roughly parallel to the bilayer surface. The difference in the magnitude and orientation of the molecular vectors results in a dipole network that is anisotropic. The orientations of nearest neighbor dipole−dipole interactions are shown by the red arrows in Figure 5B (for only one of the charged species of the molecule). It can be seen that the diagonal vectors cancel out, leaving a single net interaction between adjacent phosphate and choline groups in one axis only.

The energy associated with the nearest neighbor dipole−dipole interaction assuming that the dipoles are static, aligned, and in-plane is given by

$$W(r) = -2u^2/4\pi\varepsilon_0\varepsilon_r r^3$$

where u is the dipole moment, ε_0 the permittivity of free space, ε_r the relative permittivity of the medium, and r the dipole separation. This equates to a value of 0.13 kT, relatively small compared to that of acyl chain packing and therefore the energy associated with the second director is much smaller than the first. The calculation assumes the relative permittivity is that of water, the headgroup region being hydrated, but the exact value will depend on many factors, being in an environment of mixed composition.

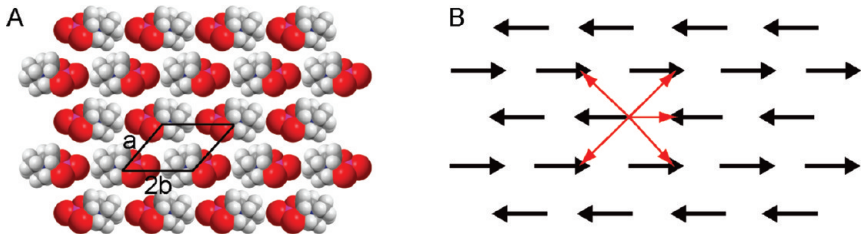

Figure 5. (A) Schematic representation of the molecular ordering of DPPC choline headgroups, formed from space-filling molecular models, showing the unit cell of the orthorhombic lattice with molecular unit cell vectors of $a = 4.6 \pm 0.3$ Å and $2b = 11.2 \pm 0.6$ Å (not to scale, phosphate group oxygen atoms in red and choline hydrogen atoms in white). (B) Corresponding organization of the molecular electric dipoles (black arrows) and illustration of nearest neighbor intermolecular dipole−dipole interactions (red arrows).

The anisotropy of the headgroup dipole network may serve to explain orientation-dependent (rotation of the bilayer plane) fluorescence emission seen in solid-phase DPPC domains when excited by polarized light at glancing incident angles seen in other studies,[27] as the orientation of the polar head-labeled fluorophore of the lipid probe is likely to be anisotropically incorporated into the headgroup dipole network in a similar manner to that of the DPPC lipid headgroups.

The range of order seen here (up to 146 nm) is in agreement with the range of ordering determined from wide-angle X-ray scattering experiments previously performed on hydrated unoriented multilamellar DPPC vesicles.[6] Our data shows that mica-supported DPPC bilayers at 23 °C exhibit mesoscopic translational and orientational headgroup order in the bilayer plane. The persistence of this positional order of the molecular headgroups over successive scans (Figure 4A,B) of the same region over a time period of tens of minutes would suggest that the lipid bilayer is in a crystalline phase. Although this seems to be in contradiction to FRAP experiments[4,5] showing finite diffusion coefficients for DPPC bilayers at similar temperatures, the difference between experiments needs to be examined more closely. Lipid diffusion coefficients measured on oriented multilamellar bilayers were 4×10^{-11} cm^2/s at 24 °C,[4] whereas those measured on oxidized silicon supports[5] were 2×10^{-12} cm^2/s, almost an order of magnitude lower. In addition to this, diffusion coefficient measurements on oxidized silicon supports showed a sharp logarithmic reduction with temperature from 32 to 24 °C, the lowest temperature measured in the study. No lateral diffusion was observed in ref 5 of substrates with only lipid monolayers formed. This would suggest that the support plays a key role in determining the lateral diffusion rate of lipids. Up to 12 layers of water have been detected by neutron reflectivity experiments between the bilayer and supporting substrate.[18,28] In addition, surface force apparatus measurements between mica surfaces in water show at least eight oscillatory force peaks, corresponding to four water layers coordinated to each mica surface.[29] Previous FM-AFM studies of DPPC bilayers[8,9] also show at least two structured water layers coordinated to DPPC headgroups. The supported DPPC bilayer will therefore be indirectly tethered to the mica substrate by a hydrogen-bonded water network which will significantly reduce lateral diffusion compared to free membranes and therefore promote orientational order, especially in gel-phase bilayers where the diffusion coefficient is already small.

We also need to take into account the proximity of the subtransition L_c to gel $L_{\beta'}$ phase boundary, which is reported to occur at 22.8 °C in one study[3] and 18.4 °C in another[1] with a half-width of 3 °C in multilamellar lipid vesicles. Our experiments at 23 °C would therefore be midtransition and thus we propose that the tendency of the mica support to structure water layers immediately adjacent to it promotes crystallization of the gel phase bilayer to the subtransition crystalline phase.

This crystalline supported bilayer would provide a very useful stable matrix for future studies examining the structure of membrane proteins incorporated into the bilayer as well as the structural interactions between the membrane proteins and the lipid molecules forming the bilayer. Given the relatively slow scan speeds of the current equipment (typically 4 min/image), however, imaging of the dynamic activity of such membrane proteins would not be possible. Many advances in AFM imaging speed have been made over the past decade, however,[30−33] which have recently enabled the light-induced conformational change of mutant bacteriorhodopsin molecules to be observed at an imaging speed of one frame per second.[34]

This study demonstrates the recent advance in the scan range of submolecular scale AFM imaging under physiologically relevant conditions that, in concert with recent advances in AFM imaging speed[30−33] and force imaging techniques,[35,36] provides much promise for the future study of biological surfaces.

AUTHOR INFORMATION

Corresponding Author
*E-mail: khizar.sheikh@ucd.ie.

ACKNOWLEDGMENT

We thank M. Klonowski, T. DuPar, and J. Cleveland of Asylum Research Inc. for their support of low noise AFM development. This work was supported by Science Foundation Ireland (07/IN.1/B931).

REFERENCES

(1) Chen, S. C.; Sturtevant, J. M.; Gaffney, B. J. *Proc. Natl. Acad. Sci. U.S.A.* **1980**, *77*, 5060–5063.
(2) Ruocco, M. J.; Shipley, G. G. *Biochim. Biophys. Acta* **1982**, *684*, 59–66.
(3) Ruocco, M. J.; Shipley, G. G. *Biochim. Biophys. Acta* **1982**, *691*, 309–320.
(4) Fahey, P. F.; Webb, W. W. *Biochemistry* **1978**, *17*, 3046–3053.
(5) Tamm, L. K.; McConnell, H. M. *Biophys. J.* **1985**, *47*, 105–113.
(6) Sun, W.-J.; Suter, R. M.; Knewtson, M. A.; Worthington, C. R.; Tristram-Nagle, S.; Zhang, R.; Nagle, J. F. *Phys. Rev. E* **1994**, *49*, 4665–4676.
(7) Fukuma, T.; Jarvis, S. P. *Rev. Sci. Instrum.* **2006**, *77*, 043701.
(8) Fukuma, T.; Higgins, M. J.; Jarvis, S. P. *Biophys. J.* **2007**, *92*, 3603–3609.

(9) Fukuma, T.; Higgins, M. J.; Jarvis, S. P. *Phys. Rev. Lett.* **2007**, *98*, 106101.
(10) Kilpatrick, J. I.; Gannepalli, A.; Cleveland, J. P.; Jarvis, S. P. *Rev. Sci. Instrum.* **2009**, *80*, 023701.
(11) Hutter, J. L.; Bechhoefer, J. *Rev. Sci. Instrum.* **1993**, *64*, 1868–1873.
(12) See Asylum Research Inc. MFP-3D AFM manual, version 04−08 at https://support.asylumresearch.com/forum/content.php.
(13) Sader, J. E.; Jarvis, S. P. *Appl. Phys. Lett.* **2004**, *84*, 1801–1803.
(14) Kawai, S.; Kitamura, S.; Kobayashi, D.; Meguro, S.; Kawakatsu, H. *Appl. Phys. Lett.* **2005**, *86*, 193107.
(15) Sugimoto, S.; Innami, S.; Abe, M; Custance, O; Morita, S. *Appl. Phys. Lett.* **2007**, *91*, 093120.
(16) Kawai, S.; Kawakatsu, H. *Appl. Phys. Lett.* **2006**, *88*, 133103.
(17) Mingeot-Leclercq, M-P; Deleu, M.; Brasseur, R.; Dufrêne, Y. F. *Nat. Protoc.* **2008**, *3*, 1654–1659.
(18) Mou, J.; Yang, J.; Shao, Z. *J. Mol. Biol.* **1995**, *248*, 507–512.
(19) Garcia-Manyes, S.; Oncins, G.; Sanz, F. *Biophys. J.* **2005**, *89*, 4261–4274.
(20) Büldt, G.; Gally, H. U.; Seelig, A.; Seelig, J.; Zaccai, G. *Nature* **1978**, *271*, 182–184.
(21) Koenig, B. W.; Krueger, S.; Orts, W. J.; Majkrzak, C. F.; Berk, N. F.; Silverton, J. V.; Gawrisch, K. *Langmuir* **1996**, *12*, 1343–1350.
(22) Niemelä, P.; Hyvönen, M. T.; Vattulainen, I. *Biophys. J.* **2004**, *87*, 2976–2989.
(23) Raudino, A.; Mauzerall, D. *Biophys. J.* **1986**, *50*, 441–449.
(24) Von Tscharner, V.; McConnell, H. M. *Biophys. J.* **1981**, *36*, 409–419.
(25) Tristram-Nagle, S.; Zhang, R.; Suter, R. M.; Worthington, C. R.; Sun, W. −J.; Nagle, J. F. *Biophys. J.* **1993**, *64*, 1097–1109.
(26) Tu, K.; Tobias, D. J.; Blasie, J. K.; Klein, M. L. *Biophys. J.* **1996**, *70*, 595–608.
(27) Moy, V. T.; Keller, D. J.; Gaub, H. E.; McConnell, H. M. *J. Phys. Chem.* **1986**, *90*, 3198–3202.
(28) Johnson, S. J.; Bayer, T. M.; McDermott, D. C.; Adam, G. W.; Rennie, A. R.; Thomas, R. K.; Sackmann, E. *Biophys. J.* **1991**, *59*, 289–294.
(29) Israelachvili, J. N.; Pashley, R. M. *Nature* **1983**, *306*, 249–250.
(30) Ando, T.; Kodera, N.; Takai, E.; Maruyama, D.; Saito, K.; Toda, A. *Proc. Natl. Acad. Sci. U.S.A.* **2001**, *98*, 12468–12472.
(31) Ando, T.; Uchihashi, T; Fukuma, T. *Prog. Surf. Sci.* **2008**, *83*, 337–437.
(32) Hansma, P. K.; Schitter, G.; Fantner, G. E.; Prater, C. *Science* **2006**, *314*, 601–602.
(33) Fantner, G. E.; Schitter, G.; Kindt, J. H.; Ivanov, T.; Ivanova, K.; Patel, R.; Holten-Anderson, N.; Adams, J.; Thurner, P. J.; Rangelow, I. W.; Hansma, P. K. *Ultramicroscopy* **2006**, *106*, 881–887.
(34) Shibata, M.; Yamashita, H.; Uchihashi, T.; Kandori, H.; Ando, T. *Nat. Nanotechnol.* **2010**, *5*, 208–212.
(35) Nussio, R. N.; Lowe, R. D.; Voelcker, N. H.; Flavel, B. S.; Gibson, C. T.; Sykes, M. J.; Miners, J. O.; Shapter, J. G. *Soft Matter* **2010**, *6*, 2193–2199.
(36) Kimura, K.; Ido, S; Oyabu, N.; Kobayashi, K.; Hirata, Y.; Imai, T.; Yamada, H. *J. Chem. Phys.* **2010**, *132*, 194705.